optica

Perfect optics with imperfect components

David A. B. Miller

Ginzton Laboratory, Spilker Building, Stanford University, 348 Via Pueblo Mall, Stanford, California 94305-4088, USA (dabm@ee.stanford.edu)

Received 15 April 2015; revised 4 June 2015; accepted 18 June 2015 (Doc. ID 238159); published 18 August 2015

Many advanced optical functions, including spatial mode converters, linear optics quantum computing gates, and arbitrary linear optical processors for communications and other applications could be implemented using meshes of Mach–Zehnder interferometers in technologies such as silicon photonics, but performance is limited by beam splitters that deviate from the ideal 50:50 split. We propose a new architecture and a novel self-adjustment approach that automatically compensate for imperfect fabricated split ratios anywhere from 85:15 to 15:85. The entire mesh can be both optimized and programmed after initial fabrication, with progressive algorithms, without calculations or calibration, and even using only sources and detectors external to the mesh. Hence, one universal field-programmable linear array optical element could be mass fabricated, with broad process tolerances, and then configured automatically for a wide range of complex and precise linear optical functions.

OCIS codes: (230.3120) Integrated optics devices; (060.1810) Buffers, couplers, routers, switches, and multiplexers; (130.6750) Systems.

http://dx.doi.org/10.1364/OPTICA.2.000747

Advanced optical functions, such as arbitrary spatial mode converters for telecommunications [1–5], linear optical quantum computing gates and circuits [6–14], and other nontraditional optics [15], are challenging to design and implement. Attempts to make arbitrary unitary optical processors [8] have shown notable successes in waveguide C-NOT gates, for example [6,7,10,13,14]. Accurately setting the required calculated component values is challenging, however, and both performance and any increased functionality are limited by fabrication and calibration precision [12].

Recent work [5,15–19] has, however, shown that, with meshes of perfect Mach–Zehnder interferometers (MZIs) in technologies such as silicon photonics, we could implement any spatial linear optical function of a given dimensionality, including nonunitary transformations. Furthermore, we could automatically design or even adaptively self-configure such a mesh [17–19]. Such self-configuration allows specific applications like self-aligning beam couplers and laser beam power combiners [18]; polarization trackers [17]; spatial mode separators [17–19], combiners [17–19], and add–drop multiplexers [5]; and systems that can automatically find the best orthogonal channels through a linear optical system [19].

Many design, calibration, and setup difficulties for arbitrary finite-dimensional linear networks can be avoided using such self-configuring approaches. Such approaches work by training the network using desired optical inputs and outputs together with a succession of simple single-parameter feedback loops that set up component values one by one by minimizing or maximizing power on photodetectors. The photodetectors can be inside the mesh [17,18] or external to it (see Supplement 1, Section 4 and [18] Appendix B). This training automatically designs the network without component calibration, calculations, or multiparameter iteration, and allows adaptation to the problem of interest.

Unfortunately, actual beam-splitter ratios inside MZIs may differ significantly from the perfect 50:50 split [12,13], preventing large systems from working properly even when using these self-configuring approaches. Here we show how to relax even that requirement.

First, presuming we have some way of adjusting the beam splitters, we show how to set them up using a "beam splitter 50:50 setup algorithm" (BFSA) to be 50:50 in a MZI based only on maximizing or minimizing power on a detector; importantly, this approach does not require that we have calibrated or balanced photodetectors that directly measure the split ratio itself.

Second, we show that, with a double Mach–Zehnder interferometer (DMZI) configuration, we can use fixed fabricated split ratios that can vary anywhere from 85:15 to 15:85; after an automated setup, the DMZI operates as if it were a perfect MZI with 50:50 beam-splitter ratios.

Third, using a "mesh 50:50 setup algorithm" (MFSA) we show that this operation can be performed sequentially on an entire connected interferometer mesh, even using only detectors external to the mesh. After such a mesh setup process, we can then use the self-configuring approaches [17,18] to program the actual function we want the now-"perfect" interferometer mesh to perform.

Hence, we can consider mass fabrication of complex linear interferometer meshes, with relaxed tolerances and without precise calibration; the resulting devices can then be automatically set up in the field as arbitrary field-programmable linear array (FPLA) processors for any linear function. All of these adjustments and programming use progressive, noniterative algorithms based only on minimizing (or, alternatively, maximizing) power on detectors, without calibration of any components.

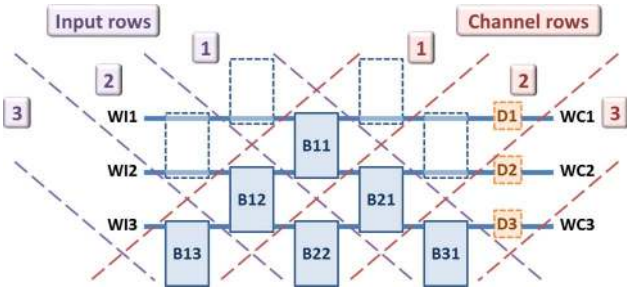

Fig. 1. Arbitrary 3 × 3 unitary transformer based on MZI blocks B*ij* as described in Fig. 2, with input (WI*i*) and output or "channel" (WC*j*) waveguides. The dashed boxes represent optional "dummy" blocks set to the "bar" (straight-through) state that could be added for greater equality of loss or phase delay. The detectors D1–D3 are optional, depending on whether detectors are included within the blocks.

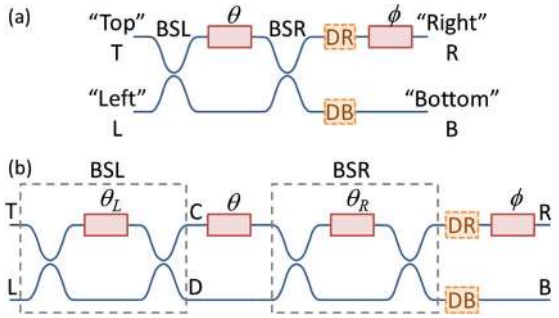

Fig. 2. MZI block configurations. (a) "Top," "Bottom," "Left," and "Right" label waveguides in correspondence with the faces of a conventional cube beam splitter. BSL and BSR are the nominally 50:50 beam splitters. The fabricated split ratios of all beam splitters may differ from this ideal split ratio. DR and DB are optional detectors, which will be mostly transparent, sampling a small amount of the power in their respective waveguides to give the signal for the feedback loops used to set up the block's function. (b) shows those beam splitters themselves implemented with additional MZIs that may also include beam splitters with fabricated split ratios unintentionally different from 50:50.

We now understand that arbitrary linear optical functions or transformations of a given dimensionality M—i.e., the equivalent of an arbitrary $M \times M$ matrix—can be implemented using interferometer meshes [17]. Figure 1 shows a mesh configuration for an example 3 × 3 unitary operation [17,18].

The input is the vector of optical amplitudes at some wavelength in the input waveguides WI*i*. (For mode converters, the actual beam may be sampled in segments, e.g., by grating couplers, into such waveguides [17,18].) The mesh multiplies this vector by a unitary matrix defined by the split ratios and phase shifts in the MZI blocks B*ij*, which can be set by training [17,18], giving an output vector as the amplitudes in the channel waveguides WC*j*. For nonunitary operations, the channel waveguides are fed through modulators to another such unitary block run backwards [17,18] to give final outputs. Addition of optional dummy MZI blocks, as shown in Fig. 1, means that all beams interfering on the photodetectors used in feedback loops have passed through the same number of MZIs; hence, if the loss is the same in all the MZIs, the total loss is equal on all such paths, giving a unitary transform that is "perfect" within an overall loss factor.

Figure 2 shows example MZI block implementations (see also Supplement 1, Section 1). These MZI blocks include phase shifters of angle θ to control the split ratio of the MZI and ϕ to control an additional phase. We expect now that the "left" (BSL) and "right" (BSR) beam splitters inside the MZI have fabricated power "reflectivities" $R_L = |r_L|^2$ and $R_R = |r_R|^2$, respectively (for field "reflectivities" r_L and r_R, respectively), that possibly differ from 50%. ("Reflectivity" here means the fraction of the top left input that appears at the upper right output for a given beam splitter or MZI.)

We presume we have some physical way of adjusting the split ratios of beam splitters BSL and BSR (both up and down) after initial fabrication. This could be some trimming of the beam splitters themselves (see Supplement 1, Section 4); alternatively, we could use the DMZI configuration of Fig. 2(b) in which the beam splitters are implemented with additional MZIs that may themselves be made with imperfect beam splitters.

Now we construct an algorithm, based only on minimizing or maximizing power in detectors DB or DR, that allows us to set BSL and BSR to 50:50 beam-splitting ratios, without calibrating any component.

Defining the reflectivity differences compared to 50%, $\delta R_L = R_L - 1/2$ and $\delta R_R = R_R - 1/2$, then, for unit input power in a coherent beam into the "top" port T, the power emerging from the "right" R port is, by a straightforward analysis of such a device,

$$P_R = \frac{1}{2} + 2\left\{\delta R_L \delta R_R - \left[\left(\frac{1}{4} - \delta R_L^2\right)\left(\frac{1}{4} - \delta R_R^2\right)\right]^{1/2} \cos\theta\right\}. \quad (1)$$

θ here includes all the phase differences between the two paths inside the interferometer, and we presume the positive square root. For simplicity, we presume that changing δR_L (or δR_R) does not change the relative phase of the resulting beams in the interferometer arms (though we can handle such phases changes—See Supplement 1, Section 2).

Note in Eq. (1), independent of δR_L and δR_R, that the power in detector or monitoring point DR is minimized for the same choice of phase θ—here a choice such that $\cos\theta = 1$ (e.g., $\theta = 0$)—giving

$$P_{R\,min} = \frac{1}{2} + 2\left\{\delta R_L \delta R_R - \left[\left(\frac{1}{4} - \delta R_L^2\right)\left(\frac{1}{4} - \delta R_R^2\right)\right]^{1/2}\right\}. \quad (2)$$

Such a choice also maximizes the power at output B, with $P_{B\,max} = 1 - P_{R\,min}$; this choice of θ is therefore attempting to put the interferometer in its best version of a "cross" state given the actual values of δR_L and δR_R.

The power at output R is maximized by choosing a phase θ such that $\cos\theta = -1$ (e.g., $\theta = \pi$), giving

$$P_{R\,max} = \frac{1}{2} + 2\left\{\delta R_L \delta R_R + \left[\left(\frac{1}{4} - \delta R_L^2\right)\left(\frac{1}{4} - \delta R_R^2\right)\right]^{1/2}\right\}. \quad (3)$$

The condition for maximum power in output R also corresponds to minimum power $P_{B\,min}$ in output B, with $P_{B\,min} = 1 - P_{R\,max}$; this choice of θ is therefore attempting to put the interferometer in its best version of a "bar" state given the actual values of δR_L and δR_R.

The function $1 - P_{R\,max} = P_{B\,min}$ (which is easier to visualize than $P_{R\,max}$) is graphed in Fig. 3(a), showing a minimum of zero (so a maximum in $P_{R\,max}$) along the line $\delta R_L = \delta R_R$. The graph

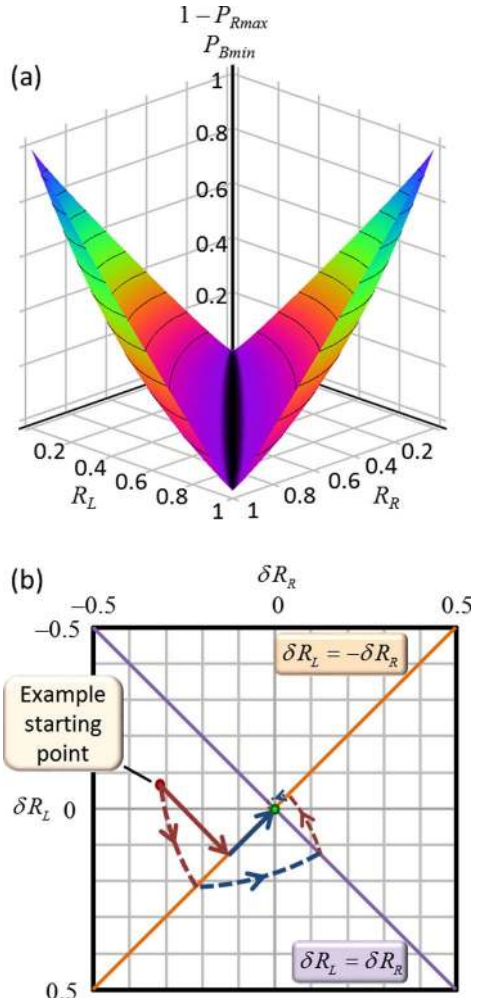

Fig. 3. (a) $1 - P_{R\,max}(R_L, R_R)$ [or, equivalently, $P_{B\,min}(R_L, R_R)$]. (b) Convergence of 50:50 alignment algorithm. The diagonal lines represent the expressions $\delta R_L = \delta R_R$ and $\delta R_L = -\delta R_R$ that correspond to the minimums of $1 - P_{R\,max}(R_L, R_R)$ and $P_{R\,min}(R_L, R_R)$, respectively.

of $P_{R\,min}(R_L, R_R)$ (Supplement 1, Fig. S2) is essentially identical but rotated by 90° in the (R_L, R_R) plane, with its minimum of zero along the line $\delta R_L = -\delta R_R$. These straight lines are sketched in Fig. 3(b).

The extinction ratio for the "bar" and "cross" states can be written as $P_{R\,max}/P_{B\,min}$ and $P_{B\,max}/P_{R\,min}$, respectively. Note that, for the interferometer to allow both extinction ratios to approach the "perfect" condition of being arbitrarily large, we require $\delta R_L = \delta R_R = 0$, i.e., 50:50 beam splitters, which corresponds to the point in the center of Fig. 3(b), where the straight lines cross.

These lines and the convex properties of the functions $P_{R\,max}(R_L, R_R)$ and $P_{R\,min}(R_L, R_R)$ allow an algorithm, based only on minimizing and maximizing powers at DR, that sets both δR_L and δR_R to zero, thereby making both beam splitters have a 50:50 split ratio.

This BFSA proceeds as follows. We shine a constant power only into the "top" T port throughout the algorithm.

(1) Set the phase shift θ to minimize the power at DR.
(2) Adjust δR_L and δR_R together, in the same sense (ideally by equal amounts) to minimize the power at DR.
(3) Set the phase shift θ to maximize the power at DR.
(4) Adjust δR_L and δR_R together, but in the opposite sense (ideally by equal but opposite amounts) to maximize the power at DR.
(5) Repeat Steps (1)–(4) if necessary until the minimum power in Step (2) is zero (or as small as can be attained) and the maximum power in Step (4) is 1 (or as large as can be attained).

[We could also run this algorithm using detector DB, minimizing power ($P_{B\,min}$) at DB in Steps (3) and (4), and/or maximizing power ($P_{B\,max}$) at DB in Steps (1) and (2).]

We can see why this works by looking at Fig. 3(b). In the ideal case (solid straight arrows), where we can change δR_L and δR_R by exactly equal amounts for Step (2) and by exactly equal and opposite amounts in Step (4), this algorithm will converge in one pass through Steps (1)–(4). In a more general case (curved dashed lines), as long as the sense of the relative changes is correct in the simultaneous adjustments of δR_L and δR_R in Steps (2) and (4), the algorithm can converge in multiple passes.

For the DMZI implementation, as long as we keep θ_L and θ_R both within a range, such as 0 to π, so that cos θ_L and cos θ_R are both monotonic in the same sense throughout, we would make same-sense adjustments of θ_L and θ_R to change δR_L and δR_R in the same sense for Step (2) and make opposite-sense adjustments of θ_L and θ_R to change δR_L and δR_R in the opposite sense for Step (4). So, δR_L and δR_R need not change by equal or equal-but-opposite amounts as we correspondingly adjust θ_L and θ_R by approximately equal or equal-but-opposite amounts; it is only necessary that the sense or sign of the reflectivity changes is correct for the algorithm to converge.

So far we have presumed that we can adjust the left and right beam splitters BSL and BSR to be 50:50 splitters; in the DMZI implementation, we are presuming some values of θ_L and θ_R allow us to achieve this. We can use our analysis of a MZI above to understand just what range of fabricated beam-splitter ratios we can tolerate while still allowing the resulting MZIs in the DMZI configuration to function as 50:50 beam splitters after appropriate adjustment. Specifically, we can reuse the result Eq. (2) above, applying it now to the MZI that constitutes either BSL or BSR in Fig. 2(b).

Consider BSL for definiteness; now take δR_L and δR_R to refer to the fixed fabricated beam splitters within BSL and θ to refer θ_L. Our goal is to be able to set BSL to be overall a 50:50 beam splitter by adjusting θ (i.e., θ_L). So we want P_R to be ½, and, hence, from Eq. (1),

$$\delta R_L \delta R_R = \{[(1/4) - \delta R_L^2][(1/4) - \delta R_R^2]\}^{1/2} \cos\theta. \quad \textbf{(4)}$$

Squaring both sides and noting that $\cos^2\theta \le 1$ gives

$$\delta R_L^2 \delta R_R^2 \le [(1/4) - \delta R_L^2][(1/4) - \delta R_R^2], \quad \textbf{(5)}$$

which can be rearranged to give

$$\delta R_L^2 + \delta R_R^2 \le 1/4. \quad \textbf{(6)}$$

Therefore, to impose a limit on the variation δR that can be tolerated in all fabricated beam splitters, we need $\delta R^2 \le 1/8$, which in turn means

$$|\delta R| \le 1/\sqrt{8} \simeq 0.35. \quad \textbf{(7)}$$

So, as long as the fabricated power split ratio in the physical beam splitters lies in the range of 15% to 85%, there is some setting of

the phase shifter in the MZI that allows the MZI overall to behave as a 50:50 beam splitter.

Hence, even with fabricated beam-splitter ratios anywhere from 15:85 to 85:15, we can make an overall MZI block that behaves as if it had "perfect" 50:50 beam splitters, and we have shown a simple algorithm based only on power maximization or minimization that allows us to set this condition.

Finally, we can add a further progressive MFSA (Supplement 1, Section 3) that allows us to set all the blocks in the mesh using this approach. Versions of this algorithm can run using detectors either embedded in each block or only externally at the outputs.

After running the MFSA, we are then ready to configure the actual "perfect" mesh for its ultimate function using the "self-configuring linear component algorithm" (SLCA) "training" approach of Refs. [17,18]. Full versions of the above algorithms and some auxiliary algorithms are described in Supplement 1, Section 4.

Note the SLCA with embedded detectors can run continuously [17,18] with live signals, though readjusting the 50:50 split ratios requires resetting the whole system from the beginning again. Both the MFSA and SLCA are sequential, so an $M \times M$ MZI mesh requires $\sim M^2$ sequential minimization sequences for each algorithm, which may limit scalability for systems that drift in time. If adjustments each have a time constant τ, as in heating a phase shifter, we expect times of multiple τ for each such minimization in each MZI block, so for large meshes the time to configure the system may not be negligible compared to times for environmental drift.

To illustrate the range of linear operations such a FPLA element could perform, in Supplement 1, Section 5 we show various example designs that would result automatically. Unitary examples include a three-way splitter, a C-NOT gate, a Hadamard transform, a Fourier transform, and the equivalent of a lens. Nonunitary examples include spatial differentiation and integration, and power splitters.

We have shown how to set up the beam splitters in an MZI to be 50:50, and how to implement this using a DMZI configuration with fixed fabricated split ratios anywhere in the range 85:15–15:85. We presented progressive algorithms to set up entire meshes of MZIs in this fashion, thereby preparing them for subsequent programming of the actual desired arbitrary linear optical function for such a "perfect" mesh. All of these operations can be completed progressively, based only on power maximization or minimization in detectors that can even be external to the entire mesh.

Hence we have established a procedure that allows us to use mass-fabricated components with imperfect parameters to be set up in the field for arbitrary spatial linear optical functions, allowing fully FPLAs with relaxed manufacturing tolerances. Such an approach therefore suggests that, by exploiting the combination of relatively relaxed manufacture together with modest and simple automatic run-time control, we may be able to implement linear optical systems of much greater complexity and sophistication than has previously been possible, and at low cost.

Funding. Air Force Office of Scientific Research (AFOSR) (FA9550-09-0704, FA9550-12-1-0024).

See Supplement 1 for supporting content.

REFERENCES

1. D. J. Richardson, J. M. Fini, and L. E. Nelson, Nat. Photonics **7**, 354 (2013).
2. R. Ryf, S. Randel, A. H. Gnauck, C. Bolle, A. Sierra, S. Mumtaz, M. Esmaeelpour, E. C. Burrows, R.-J. Essiambre, P. J. Winzer, D. W. Peckham, A. H. McCurdy, and R. Lingle, Jr., J. Lightwave Technol. **30**, 521 (2012).
3. S. G. Leon-Saval, N. K. Fontaine, J. R. Salazar-Gil, B. Ercan, R. Ryf, and J. Bland-Hawthorn, Opt. Express **22**, 1036 (2014).
4. H. Huang, G. Xie, Y. Yan, N. Ahmed, Y. Ren, Y. Yue, D. Rogawski, M. J. Willner, B. I. Erkmen, K. M. Birnbaum, S. J. Dolinar, M. P. J. Lavery, M. J. Padgett, M. Tur, and A. E. Willner, Opt. Lett. **39**, 197 (2014).
5. D. A. B. Miller, Opt. Express **21**, 20220 (2013).
6. A. Laing and J. L. O'Brien, "Super-stable tomography of any linear optical device," arXiv:1208.2868 (2012).
7. S. Rahimi-Keshari, M. A. Broome, R. Fickler, A. Fedrizzi, T. C. Ralph, and A. G. White, Opt. Express **21**, 13450 (2013).
8. M. Reck, A. Zeilinger, H. J. Bernstein, and P. Bertani, Phys. Rev. Lett. **73**, 58 (1994).
9. J. L. O'Brien, A. Furusawa, and J. Vučković, Nat. Photonics **3**, 687 (2009).
10. P. Kok, W. J. Munro, K. Nemoto, T. C. Ralph, J. P. Dowling, and G. J. Milburn, Rev. Mod. Phys. **79**, 135 (2007).
11. J.-W. Pan, Z.-B. Chen, C.-Y. Lu, H. Weinfurter, A. Zeilinger, and M. Żukowski, Rev. Mod. Phys. **84**, 777 (2012).
12. J. Mower, N. C. Harris, G. R. Steinbrecher, Y. Lahini, and D. Englund, "Towards high-fidelity quantum computation and simulation on a programmable photonic integrated circuit," arXiv:1406.3255v2 (2014).
13. J. Mower, N. C. Harris, G. R. Steinbrecher, Y. Lahini, and D. Englund, in *Conference on Lasers and Electro-Optics* (Optical Society of America, 2014), paper FM2A.3.
14. H. W. Li, J. Wabnig, D. Bitauld, P. Shadbolt, A. Politi, A. Laing, J. L. O'Brien, and A. O. Niskanen, New J. Phys. **15**, 063017 (2013).
15. D. A. B. Miller, J. Opt. Soc. Am. A **30**, 238 (2013).
16. D. A. B. Miller, Opt. Express **20**, 23985 (2012).
17. D. A. B. Miller, Photon. Res. **1**, 1 (2013).
18. D. A. B. Miller, Opt. Express **21**, 6360 (2013).
19. D. A. B. Miller, J. Lightwave Technol. **31**, 3987 (2013).